Progress In Electromagnetics Research, PIER 34, 63–88, 2001

SCATTERING OF A PLANE WAVE BY A 1-DIMENSIONAL ROUGH SURFACE STUDY IN A NONORTHOGONAL COORDINATE SYSTEM

R. Dusséaux

Université de Versailles Saint-Quentin en Yveline
Centre d' étude des Environnements Terrestre et Planétaires (CETP), UMR 8639
10-12 Avenue de l'Europe, 78140 Vélizy, France

R. de Oliveira

Université de Versailles Saint-Quentin en Yveline
Laboratoire des Signaux et Systèmes - Supelec
Plateau de Moulon, 91192 Gif sur Yvette, France

Abstract—We present a method giving the field scattered by a plane surface with a cylindrical local perturbation illuminated by a plane wave. The theory is based on Maxwell's equations in covariant form written in a nonorthogonal coordinate system fitted to the surface profile. The covariant components of electric and magnetic vectors are solutions of a differential eigenvalue system. A Method of Moments (PPMoM) with Pulses for basis and weighting functions is applied for solving this system in the spectral domain. The scattered field is expanded as a linear combination of eigensolutions satisfying the outgoing wave condition. Their amplitudes are found by solving the boundary conditions. Above a given deformation, the Rayleigh integral is valid and becomes identified with one of covariant components of the scattered field. Applying the PPMo Method to this equality, we obtain the asymptotic field and the scattering pattern. The method is numerically investigated in the far-field zone, by means of convergence tests on the spectral amplitudes and on the power balance criterion. The theory is verified by comparison with results obtained by a rigorous method.

1. INTRODUCTION

We present a method giving the field scattered by a plane surface with a cylindrical local perturbation illuminated by a plane wave in $E_{\|}$ or $H_{\|}$ polarization. This perfectly conducting surface is defined by the equation $y = a(x)$ where $a(x)$ is a local function.

The method is based on Maxwell's equations in covariant form written in the translation system $(x, u = y - a(x), z)$ [1–4]. The covariant components of electric vector $\vec{E}$ and magnetic vector $\vec{H}$ fulfill an eigenvalue system. A Method of Moments (MoM) is applied to solve this system in the spectral domain [5]. The Fourier transforms of the covariant components of fields are expanded in series of basis functions $\hat{b}_q(\alpha)$. Using an inner product, the differential system is projected over weighting functions $\hat{w}_q(\alpha)$ and finally, a scattering matrix is obtained, the size of which is fixed by the truncation order M. The eigenvalues of this matrix and the corresponding eigenvectors lead to elementary wave functions. The scattered field is expanded as a linear combination of eigensolutions satisfying the outgoing wave condition, the amplitudes of which are found by solving the boundary conditions. Above the deformation, the Rayleigh integral [6, 7] is valid and becomes identified with one of the covariant components of the scattered field.

By applying a method of moments to this equality, we obtain the asymptotic field and the scattering pattern.

The method of curvilinear coordinates [1–3] has given rise to some work in the field of rough surfaces [8–10]. The authors have applied a "Pulse/Dirac" method of moments for solving the differential system and the boundary conditions, using piecewise functions (Pulses) of width $\Delta\alpha$, centered on $\alpha_q = q\Delta\alpha$ as basis functions, and Dirac delta functions $\delta(\alpha - \alpha_q)$ as weighting functions.

In this paper, we apply a method of moments with Pulses as basis and weighting functions. In Section 4, we present the theoretical aspects of the method. The lengthy and fastidious calculations are detailed in the appendix. In Section 5, we numerically investigate the Pulse/Pulse method of moments. The study is concerned with the convergence of spectral amplitudes and power conservation [11–13] as a function of the truncation order M and of the spectral resolution $\Delta\alpha$. Finally, we propose a comparison of scattering patterns with those obtained by a rigorous method [13, 14].

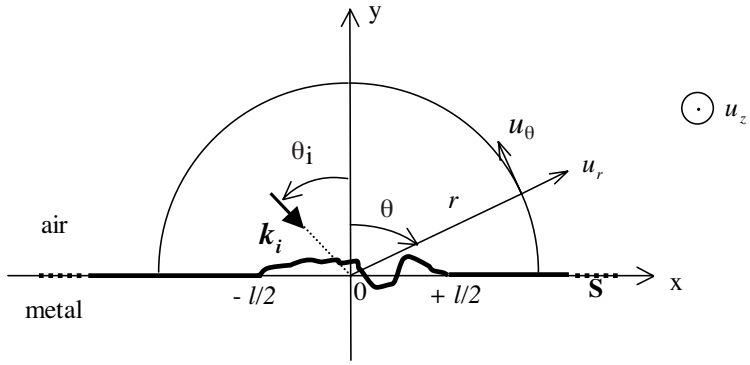

Figure 1. Plane with a local deformation illuminated by a plane wave under incidence θ_i. According to our conventions, θ_i and θ are positive here.

2. PRESENTATION OF THE PROBLEM

In Fig. 1, we consider a local perturbation in a perfectly conducting plane surface. The deformation is given by the equation $y = a(x)$, where $a(x)$ is a local function defined over the support $[-l/2; l/2]$. l is the width of the modulated zone. This structure is illuminated under incidence θ_i by a monochromatic plane wave of wavelength λ. The incident wave vector $\vec{k}_i$ lies in the xOy plane. Both fundamental cases

of polarization $E_{\parallel}$ and $H_{\parallel}$ are considered. The time-dependance factor in $\exp(j\omega t)$, where ω is the angular frequency, is suppressed.

$$F_i(x,y) = \exp(-j\alpha_i x + j\beta_i y) = \begin{cases} E_{z,i}(x,y) & \text{in } E_{\parallel} \\ ZH_{z,i}(x,y) & \text{in } H_{\parallel} \end{cases} \tag{1a}$$

$$Z = \sqrt{\frac{\mu_0}{\varepsilon_0}} \approx 120\pi; \quad \left|\vec{k}_i\right| = k = \frac{2\pi}{\lambda}; \quad \alpha_i = k\sin\theta_i; \quad \beta_i = k\cos\theta_i \tag{1b}$$

Without any deformation, the total field $F_0(x,y)$ is the sum of the incident field $F_i(x,y)$ and the specularly reflected field $F_r(x,y)$:

$$F_0(x,y) = F_i(x,y) + F_r(x,y) \tag{2a}$$

$$F_r(x,y) = \rho\exp(-j\alpha_i x - j\beta_i y) \quad \text{with } \rho = -1 \text{ for } E_{\parallel} \text{ and } \rho = 1 \text{ for } H_{\parallel} \tag{2b}$$

For a locally deformed plane, we consider, in addition to the incident and specularly reflected waves, a scattered field $F_d(x,y)$. Thus, the total field is defined as follows [6]:

$$F_t(x,y) = F_0(x,y) + F_d(x,y) \tag{3}$$

The problem consists in working out the scattered field $F_d(x,y)$.

3. RAYLEIGH INTEGRAL AND FAR FIELD

Let $y_{\max}$ be the maximum height of the deformation. For $y > y_{\max}$, $F_d(x,y)$, can be represented by a superposition of a continuous spectrum of outgoing plane waves [6, 7], the so-called Rayleigh integral (4):

$$\forall x, \forall y > y_{\max}, F_d(x,y) = \begin{cases} E_{z,i}(x,y) \text{ for } E_{\parallel} \\ \text{or} \\ ZH_{z,i}(x,y) \text{ for } H_{\parallel} \end{cases} = \frac{1}{2\pi}\int_{-\infty}^{+\infty} \hat{R}(\alpha)\exp(-j\beta(\alpha)y)\exp(-j\alpha x)d\alpha \tag{4}$$

For the propagating waves, $|\alpha| < k$ and:

$$\alpha = k\sin\theta \text{ et } \beta(\alpha) = \sqrt{k^2-\alpha^2} = k\cos\theta \text{ with } -\pi/2 < \theta < \pi/2 \tag{5a}$$

For the evanescent waves, $|\alpha| \geq k$ and:

$$\beta(\alpha) = -j\sqrt{k^2-\alpha^2} \tag{5b}$$

The Rayleigh integral in the far zone can be reduced to [11]:

$$\vec{F}_d(r,\theta) \approx \sqrt{\frac{k}{2\pi r}}\hat{R}(k\sin\theta)\cos\theta\exp(-jkr)\exp\left(j\frac{\pi}{4}\right)\vec{u}_z \qquad (6)$$

The asymptotic field decreases as $1/\sqrt{r}$ [15]. The angular dependence is given by function $R(\alpha)\cos\theta$ and becomes identified with the propagating wave amplitudes of the continuous spectrum (4) with $\alpha = k\sin\theta$.

Using expression (6), the scattered elementary power $dP_d(\theta)$ can be defined (Eq. 7):

$$\frac{dP_d(\theta)}{d\theta} = \frac{k\left|\hat{R}(\theta)\right|^2\cos^2(\theta)}{4\pi Z} \quad \text{with} \quad -\pi/2 < \theta < +\pi/2 \qquad (7)$$

$dP_d(\theta)$ is the real part of the flux of the complex scattered Poynting vector through an elementary surface $d\vec{S} = rd\theta\Delta z\vec{u}_z$ with $\Delta z = 1$. The angular power density $\frac{dP_d(\theta)}{d\theta}$ (W/rad) defines the scattering pattern.

The function $\hat{R}(\theta)$ fulfils the power balance criterion (8) [11–13] where P_d corresponds to the total scattered power and P_c represents the electromagnetic coupling between $(\vec{E}_d, \vec{H}_d)$ and $(\vec{E}_0, \vec{H}_0)$.

$$P_d = P_c \text{ with } P_d = \int_{-\pi/2}^{+\pi/2}\frac{dP_d}{d\theta}d\theta \text{ and } P_c = -\frac{\rho}{Z}\Re e\left[\hat{R}(\alpha_i)\right]\cos\theta_i \qquad (8)$$

The scattered field cannot be expressed by the Rayleigh integral in the modulated zone ($y < y_{\max}$) and the function $R(\alpha)$ cannot be found by solving the boundary conditions if the perturbation amplitude is too large [6, 7]. In this paper, we propose to obtain an expression of electromagnetic fields that is valid everywhere in space, outside and on the surface, by solving Maxwell's equations in the translation coordinates system $(x, u = y - a(x), z)$ [1, 2].

4. THEORY — METHOD OF MOMENTS IN THE SPECTRAL DOMAIN

4.1. Components of Fields and Differential System

If there is no current density and no charge density, then under their covariant form [1, 3], Maxwell's equations expressed in the translation

system lead to a differential system of the first order in u:

$$\frac{1}{jk}\frac{\partial F(x,u)}{\partial u} = \frac{d(x)}{jk}\frac{\partial F(x,u)}{\partial x} + (c(x)-1)G(x,u) \tag{9a}$$

$$\frac{1}{jk}\frac{\partial G(x,u)}{\partial u} = \frac{1}{k^2}\frac{\partial}{\partial x}\left[c(x)\frac{\partial F(x,u)}{\partial x}\right] - \frac{1}{k^2}\frac{\partial^2 F(x,u)}{\partial x^2} - F(x,u) + \frac{1}{jk}\frac{\partial}{\partial x}[d(x)G(x,u)] \tag{9b}$$

The local functions $c(x)$ and $d(x)$ depend on the profile derivative (Eq. 10).

$$d(x) = \frac{\dot{a}(x)}{1+\dot{a}(x)^2}; \qquad c(x) = \dot{a}(x)d(x); \qquad \dot{a}(x) = \frac{da(x)}{dx} \tag{10}$$

System (9) is valid for the two polarization types with

$$\text{for } E_{\parallel} \text{ polarization}: \; F(x,u) = E_z(x,u);\; G(x,u) = ZH_x(x,u) \tag{11a}$$

$$ZH_u(x,u) = G_u(x,u) = \frac{-j(1-c(x))}{k}\frac{\partial F(x,u)}{\partial x} + d(x)G(x,u)$$

$$E_x(x,u) = E_u(x,u) = H_z(x,u) = 0$$

$$\text{for } H_{\parallel} \text{ polarization}: F(x,u) = ZH_z(x,u);\; G(x,u) = -E_x(x,u) \tag{11b}$$

$$E_u(x,u) = G_u(x,u) = \frac{j(1-c(x))}{k}\frac{\partial F(x,u)}{\partial x} - d(x)G(x,u)$$

$$H_x(x,u) = H_u(x,u) = E_z(x,u) = 0$$

The covariant components $[E_x(x,u); E_z(x,u)]$ and $[H_x(x,u); H_z(x,u)]$ of electric and magnetic fields are parallel to surfaces $u = y_j$, respectively. These components verify the boundary conditions in $u = 0$, hence their presence in differential system (9).

After a positive Fourier transform [8], system (9) takes the form:

$$\frac{1}{jk}\frac{\partial \hat{F}(\alpha,u)}{\partial u} = \frac{-1}{2\pi k}\int_{-\infty}^{+\infty}\gamma\hat{d}(\alpha-\gamma)\hat{F}(\gamma,u)d\gamma + \frac{1}{2\pi}\int_{-\infty}^{+\infty}\hat{c}(\alpha-\gamma)\hat{G}(\gamma,u)d\gamma - \hat{G}(\alpha,u) \tag{12a}$$

$$\frac{1}{jk}\frac{\partial \hat{G}(\alpha,u)}{\partial u} = \frac{-\alpha}{2\pi k^2}\int_{-\infty}^{+\infty}\gamma\hat{c}(\alpha-\gamma)\hat{F}(\gamma,u)d\gamma - \frac{k^2-\alpha^2}{k^2}\hat{F}(\alpha,u)$$

$$- \frac{\alpha}{2\pi} \int_{-\infty}^{+\infty} \hat{G}(\gamma, u)\hat{d}(\alpha - \gamma)d\gamma \tag{12b}$$

$\hat{F}(\alpha, u)$, $\hat{G}(\alpha, u)$, $\hat{c}(\alpha)$ and $\hat{d}(\alpha)$ are the Fourier transforms of functions $F(x, u)$, $G(x, u)$, $c(x)$ and $d(x)$, respectively.

4.2. The Scattering Matrix

A method of moments with pulses as basis and weighting functions is applied to solve system (12) in the spectral domain [5]. The unknown functions $\hat{F}(\alpha, u)$ and $\hat{G}(\alpha, u)$ and the Fourier transforms $\hat{c}(\alpha)$ and $\hat{d}(\alpha)$ are expanded in a series of basis functions $\hat{b}_q(\alpha)$:

$$\hat{F}(\alpha, u) = \sum_{q=-\infty}^{q=+\infty} F_q(u)\hat{b}_q(\alpha) \quad ; \quad \hat{G}(\alpha, u) = \sum_{q=-\infty}^{q=+\infty} G_q(u)\hat{b}_q(\alpha) \tag{13}$$

$$\hat{c}(\alpha) = \sum_{q=-\infty}^{q=+\infty} c_q\hat{b}_q(\alpha) \quad ; \quad \hat{d}(\alpha) = \sum_{q=-\infty}^{q=+\infty} d_q\hat{b}_q(\alpha) \tag{14}$$

where $\hat{b}_q(\alpha)$ is a piecewise function (pulse) of unit amplitude, of width $\Delta\alpha$ and centered on $\alpha_q = q\Delta\alpha$. The spectral resolution $\Delta\alpha$ is defined as follows:

$$\Delta\alpha = \frac{2k}{2M_c + 1} \tag{15}$$

where M_c is the cut-off integer. The basis functions constitute an orthonormal basis referring to inner product (16) where $\delta_{m,q}$ denotes the Kronecker symbol.

$$\left\langle \hat{b}_m(\alpha); \hat{b}_q(\alpha) \right\rangle = \int_{-\infty}^{+\infty} \hat{b}_m(\alpha)\hat{b}_q(\alpha)d\alpha = \Delta\alpha\delta_{m,q} \tag{16}$$

Substituting expressions (13) and (14) into system (12) and taking the inner product of the intermediate equations with each basis function $\hat{b}_q(\alpha)$, we obtain a set of differential equations relating coefficients $F_q(\alpha)$ and $G_q(\alpha)$ to each other (17).

$$\frac{1}{jk}\frac{dF_m(u)}{du} = \sum_{q=-\infty}^{q=+\infty} L_{mq}^{(11)}F_q + L_{mq}^{(12)}G_q \tag{17a}$$

$$\frac{1}{jk}\frac{dG_m(u)}{du} = \sum_{q=-\infty}^{q=+\infty} L_{mq}^{(21)}F_q + L_{mq}^{(22)}G_q \tag{17b}$$

The calculations giving the expressions of c_q, d_q and $L_{mq}^{(ij)}$ are detailed in the appendix. The numerical solution of (17) requires a truncation order M. In Eqs. (13) and (17), the following conditions (18) are imposed.

$$L_{mq}^{(ij)} = 0 \text{ and } F_q(u) = G_q(u) = 0 \text{ if } |m| \text{ and } |q| > M \tag{18}$$

The elementary solutions of (17) are defined as follows:

$$F_m(u) = f_m \exp(jkru) \quad ; \quad G_m(u) = g_m \exp(jkru) \tag{19}$$

Thus, relationships (17) can be written in matrix form:

$$\mathbf{L} \begin{pmatrix} \vec{f} \\ \vec{g} \end{pmatrix} = \begin{bmatrix} \mathbf{L}^{(11)} & \mathbf{L}^{(12)} \\ \mathbf{L}^{(21)} & \mathbf{L}^{(22)} \end{bmatrix} \begin{pmatrix} \vec{f} \\ \vec{g} \end{pmatrix} = r \begin{pmatrix} \vec{f} \\ \vec{g} \end{pmatrix} \tag{20}$$

With the M^{th}-order truncated approximation, the scattering matrix $\mathbf{L}$ is $(4M+2)$-dimensional. Vectors $\vec{f}$ and $\vec{g}$ have components f_m and g_m with $-M < m < M$. The resolution gives $4M+2$ vectors $\vec{f}_n$ and $\vec{g}_n$ corresponding to $4M+2$ eigenvalues r_n of $\mathbf{L}$. Finally, the eigensolutions of initial system (12) take the following form:

$$\begin{aligned} \hat{F}_n(\alpha, u) &= \sum_{q=-M}^{q=+M} f_{qn} \hat{b}_q(\alpha) \exp(jkr_n u) \text{ with } 1 \le n \le 4M+2 \\ \hat{G}_n(\alpha, u) &= \sum_{q=-M}^{q=+M} g_{qn} \hat{b}_q(\alpha) \exp(jkr_n u) \end{aligned} \tag{21}$$

4.3. Properties of the Scattering Matrix and of the Eigenvalue Spectrum

Matrices $\mathbf{L^{(21)}}$ and $\mathbf{L^{(12)}}$ are hermitian and the hermitian transpose of $\mathbf{L^{(11)}}$ is $\mathbf{L^{(22)}}$. Thus, the hermitian transpose $\mathbf{L^{HT}}$ of the scattering matrix $\mathbf{L}$ is given by:

$$\mathbf{L^{HT}} = \begin{bmatrix} \mathbf{L^{(22)}} & \mathbf{L^{(12)}} \\ \mathbf{L^{(21)}} & \mathbf{L^{(11)}} \end{bmatrix} \quad \text{and} \quad \mathbf{L^{HT}} \begin{pmatrix} \vec{g}_n \\ \vec{f}_n \end{pmatrix} = r_n \begin{pmatrix} \vec{g}_n \\ \vec{f}_n \end{pmatrix} \tag{22}$$

According to (22), the eigenvalues of $\mathbf{L^{HT}}$ are identical to those of $\mathbf{L}$. Moreover, if r_n is an eigenvalue of $\mathbf{L}$, the conjugate eigenvalue r_n^* is an eigenvalue of $\mathbf{L^{HT}}$. Consequently, r_n^* is also an eigenvalue of the scattering matrix. This property have been already shown for the diffraction grating studied in the translation system [16, 17].

Let $\mathbf{L_{180}^{(ij)}}$ the matrix obtained through a 180-degree rotation of the elements in matrix $\mathbf{L^{(ij)}}$. Using the hermitian symmetry of c_q and d_q ($\forall q,\ c_q = c_{-q}^*$ and $d_q = d_{-q}^*$) within the expressions of coefficients $L_{qm}^{(ij)}$ (A7) given in the appendix, we show that the matrix $\mathbf{L_{180}}$ is of the form:

$$\mathbf{L_{180}} = \begin{bmatrix} -\mathbf{L^{(11)}} & \mathbf{L^{(12)}} \\ \mathbf{L^{(21)}} & -\mathbf{L^{(22)}} \end{bmatrix}^* \tag{23}$$

Combining Eq. (20) and Eq. (23), the following property is shown:

$$\mathbf{L} \begin{pmatrix} \vec{f}_{180,n}^* \\ -\vec{g}_{180,n}^* \end{pmatrix} = -r_n^* \begin{pmatrix} \vec{f}_{180,n}^* \\ -\vec{g}_{180,n}^* \end{pmatrix} \tag{24}$$

where $\vec{h}_{180,n}$ is obtained through a 180-degree rotation of the elements in vector $\vec{h}_n$. Insofar as r_n, r_n^* and $-r_n^*$ are eigenvalues, it can be deduced that the eigenvalues of the scattering matrix are opposite two by two.

The signs of the real and imaginary parts of r_n define the nature of the wave corresponding to the elementary wave function (21). In particular, $\hat{F}_n(\alpha, u)$ and $\hat{G}_n(\alpha, u)$ represent a propagating wave if $\mathrm{Re}(r_n) < 0$ and $\mathrm{Im}(r_n) = 0$ and an evanescent wave if $\mathrm{Im}(r_n) > 0$. Since r_n and $-r_n$ are eigenvalues of $\mathbf{L}$, among the $4M+2$ eigenfunctions, there are $2M+1$ of them that correspond to outgoing waves and as many of them to incoming waves.

For an infinite plane mirror, $\mathbf{L^{(12)}}$ and $\mathbf{L^{(21)}}$ are diagonal matrices; $\mathbf{L^{(11)}}$ and $\mathbf{L^{(22)}}$, null matrices. In this case, it is shown in the appendix that the eigenvalues $r_n^{(0)}$ are given by the following analytical formula (25)

$$r_n^{(0)} = \pm\sqrt{1 - P_n} \tag{25a}$$

$$P_n = \left\langle \hat{b}_n(\alpha), \frac{\alpha^2}{k^2}\hat{b}_n(\alpha) \right\rangle = \frac{12n^2+1}{3(2M_c+1)^2} \tag{25b}$$

For a pair of parameters $(M_C; M)$ with $a(x) = 0$, according to (25), there are $4M_C + 2$ real eigenvalues smaller than 1 and $4M - 4M_C$ pure imaginary eigenvalues.

For a plane surface with a local deformation, it can be noted numerically that there are $4M_C + 2$ real eigenvalues and $4M - 4M_C$ complex eigenvalues which are not necessarily purely imaginary. Depending on whether M is a sufficiently large number, the real values

r_n of the truncated matrix correspond to the reference real eigenvalues $r_n^{(0)}$.

The elementary wave functions are sorted out according to sign and value of real and imaginary parts of the corresponding eigenvalues. For all the configurations analyzed with the PPMo method, real eigenvalues have numerical imaginary parts, the absolute values of which are less than 10^{-10}. The wave functions are straightforwardly sorted into propagating and evanescent ones. Moreover, since eigenvalues are opposite two by two, the sorting of wave functions into outgoing and incoming waves can be performed without problems.

4.4. Scattering Field and Angular Power Density

The scattered field (Eq. 26) is defined as a linear combination of $2M+1$ eigensolutions satisfying the outgoing wave condition (21). According to the spectrum of eigenvalues, the scattered field is described by $2M_C+1$ eigenfunctions associated with propagating waves, and $2M-2M_C$ with evanescent waves.

$$\hat{F}_d(\alpha,u) = \sum_{n=1}^{2M+1} A_n \hat{F}_n(\alpha,u) \tag{26a}$$

$$\hat{G}_d(\alpha,u) = \sum_{n=1}^{2M+1} A_n \hat{G}_n(\alpha,u) \tag{26b}$$

The unknown amplitudes A_n are found by solving the boundary conditions (27) with the PPMo method. These conditions indicate that the tangential component of the total electric field, $F_t(x,u)$ for the case $E_\parallel$ and $G_t(x,u)$ for the $H_\parallel$ case, is zero on the perfectly conducting surface at $u=0$. It should be reminded that function $F_0(x,y)$ describes the Oz component of the total field above a plane surface (Eqs. 1 and 2). For the $H_\parallel$ polarization, $G_0(x,y)$ is the electric component associated with the magnetic component $F_0(x,y)$ and parallel to $u=0$. The minus sign in (27b) derives from relation (11b).

For $E_\parallel$ polarization:

$$F_d(x,u=0) + F_0(x,y=a(x)) = 0 \tag{27a}$$

For $H_\parallel$ polarization:

$$G_d(x,u=0) - G_0(x,y=a(x)) = 0 \tag{27b}$$

with

$$G_0(x,y) = \frac{1}{jk}\frac{\partial F_0(x,y)}{\partial y} - \dot{a}(x)\frac{1}{jk}\frac{\partial F_0(x,y)}{\partial x} \tag{27c}$$

After a Fourier transform, the continuity relations (27a–b) are projected onto the basis functions. According to (1), (2), (16), (21) and (26), for each polarization, a $(2M+1)$-dimensional matrix system (28–29) is obtained, the inversion of which leads to spectral amplitudes A_n, and thus, to $\hat{F}_d(\alpha, u)$ and $\hat{G}_d(\alpha, u)$.

For $E_{\|}$ polarization:

$$\sum_{n=1}^{2M+1} A_n f_{mn} = S_m \qquad \text{with} \qquad -M < m < +M \tag{28a}$$

and

$$S_m = -\frac{2j}{\Delta\alpha} \int_{-l/2}^{l/2} \sin(\beta_i a(x)) I_{0m}^*(x) \exp(-j\alpha_i x) dx \tag{28b}$$

For $H_{\|}$ polarization:

$$\sum_{n=1}^{2M+1} A_n g_{mn} = T_m \qquad \text{with} \qquad -M < m < +M \tag{29a}$$

and

$$T_m = \frac{2Z}{jk\beta_i \Delta\alpha} \int_{-l/2}^{+l/2} \left(k^2 I_{0m}^*(x) - \alpha_i I_{1m}^*(x)\right) \sin(\beta_i a(x)) \exp(-j\alpha_i x) dx \tag{29b}$$

Functions $I_{0m}(x)$ and $I_{1m}(x)$ are obtained by computing the following integrals:

$$I_{0m}(x) = \int_{\alpha_m - \Delta\alpha/2}^{\alpha_m + \Delta\alpha/2} \exp(-j\alpha x) d\alpha = \Delta\alpha \sin c\left(\Delta\alpha \frac{x}{2}\right) \exp(-j\alpha_m x) \tag{30a}$$

$$\begin{aligned} I_{1m}(x) &= \int_{\alpha_m - \Delta\alpha/2}^{\alpha_m + \Delta\alpha/2} \alpha \exp(-j\alpha x) d\alpha \\ &= \frac{\Delta\alpha \exp(-j\alpha_m x)}{jx} \\ &\quad \cdot \left(2j\alpha_m \sin\left(\Delta\alpha \frac{x}{2}\right) + \Delta\alpha \sin c\left(\Delta\alpha \frac{x}{2}\right) - \Delta\alpha \cos\left(\Delta\alpha \frac{x}{2}\right)\right) \end{aligned} \tag{30b}$$

The angular power density (APD) is defined from the scattering amplitudes $\hat{R}(\alpha)$ associated with the Rayleigh integral (Eqs. 4 and 7). Above the deformation, this integral (4) is valid and becomes identified with the covariant component $F_d(x, y)$ (11). At $y = y_{\max}$,

$$\forall x, F_d(x,\, u = y_{\max} - a(x)) = \frac{1}{2\pi} \int_{-\infty}^{+\infty} \hat{R}(\alpha) \exp(-j\beta(\alpha) y_{\max}) \exp(-j\alpha x) d\alpha \quad (31)$$

The function $\hat{R}(\alpha)$ is obtained by solving the continuity relation (31) with the PPMo method in the spectral domain. $\hat{R}(\alpha)$ and $\beta(\alpha)$ are expanded in a series of $\hat{b}_q(\alpha)$. (Imag(β_q) denotes the imaginary part of β_q).

$$\hat{R}(\alpha) = \sum_{q=-M}^{+M} R_q \hat{b}_q(\alpha) \quad (32)$$

$$\beta(\alpha) = \sum_{q=-M}^{+M} \beta_q \hat{b}_q(\alpha) \quad \text{with} \quad \text{Imag}(\beta_q) \leq 0 \quad (33a)$$

and

$$\beta_q = k\sqrt{1 - P_q} \quad (33b)$$

Finally, the scattering coefficients R_q are given by:

$$R_q = \frac{\exp(+j\beta_q y_{\max})}{\Delta\alpha} \sum_{n=1}^{2M+1} (V_{qn} + f_{qn}) \exp(jkr_n y_{\max}) A_n \quad (34a)$$

with

$$V_{qn} = \sum_{m=-M}^{+M} f_{mn} \int_{-l/2}^{l/2} (\exp(jkr_n a(x)) - 1) I^*_{om}(x) I_{oq}(x) dx \quad (34b)$$

The method of curvilinear coordinates [1–3] has given rise to some work in the field of rough surfaces [8–10]. The authors have applied a "Pulse/Dirac" method of moments for solving the differential system and the boundary conditions, using Pulses as basis functions and Dirac delta functions as weighting functions.

With respect to this previous work, a new formulation of the method of moments is applied using Pulses as basis and weighting functions, a new scattering matrix is generated and it is proven that

the associated eigenvalues are opposite two by two. Moreover, in refs. [8–10], the authors define the asymptotic scattered field as a plane wave expansion, even inside the modulated zone. The eigenfunctions (21) are only used to describe the evanescent field. In order to obtain the far field, we use the validity of the Rayleigh integral above the perturbation and we treat the continuity relation (31).

In this paper, no comparison is performed in terms of trade-off of accuracy versus computation time between the different solving methods (PPMoM, PDMoM and DDMoM) and relationships transforming one formulation into another one are not presented. The latter two aspects will be the object of a future publication.

5. RESULTS

5.1. Convergence Tests

M_C and M are the two numerical parameters of the method. The cut-off integer M_C sets the width $\Delta\alpha$ of pulses $\hat{b}_q(\alpha)$. As M_C increases, $\Delta\alpha$ decreases and the approximation of functions $\hat{F}_d(\alpha, u)$, $\hat{G}_d(\alpha, u)$, $\hat{c}(\alpha)$ and $\hat{d}(\alpha)$ in series (13) and (14) becomes more accurate. With the M^{th}-order truncation, the scattered field (26) is described by $2M_C + 1$ eigenfunctions associated with propagating waves, and $2M - 2M_C$ with evanescent waves. The evanescent waves contribute to the near field and take part in the coupling between propagating waves. The consequence of the M^{th}-order truncation is the suppression of high spatial frequency evanescent waves in the Fourier transform of field components (13) and in Rayleigh integral (4). Indeed, integration variable α varies within $[-\alpha_{\max}; +\alpha_{\max}]$ as follows:

$$\alpha_{\max} = \alpha_m = M\Delta\alpha = \frac{2kM}{2M_C + 1} \approx k\frac{M}{M_C} \quad \text{if} \quad M_c \gg 1 \tag{35}$$

$\alpha_{\max}$ depends on the ratio M/M_C. The proportion of the evanescent wave functions is larger when M/M_C increases, so that the coupling phenomena are better described.

If our method is numerically stable, the accuracy of the results must increase with increasing M and M_C. To illustrate this idea, a measure of error [18] is defined as follows:

$$\Delta R_n(M, M_C) = -\log_{10}\left(\left|\frac{R_n(M, M_C) - R_n(M-1, M_C)}{R_n(M, M_C)}\right|\right) \tag{36}$$

$$\Delta P(M, M_c) = -\log_{10}\left(\left|\frac{P_d(M, M_c) - P_c(M, M_c)}{P_d(M, M_c)}\right|\right) \tag{37}$$

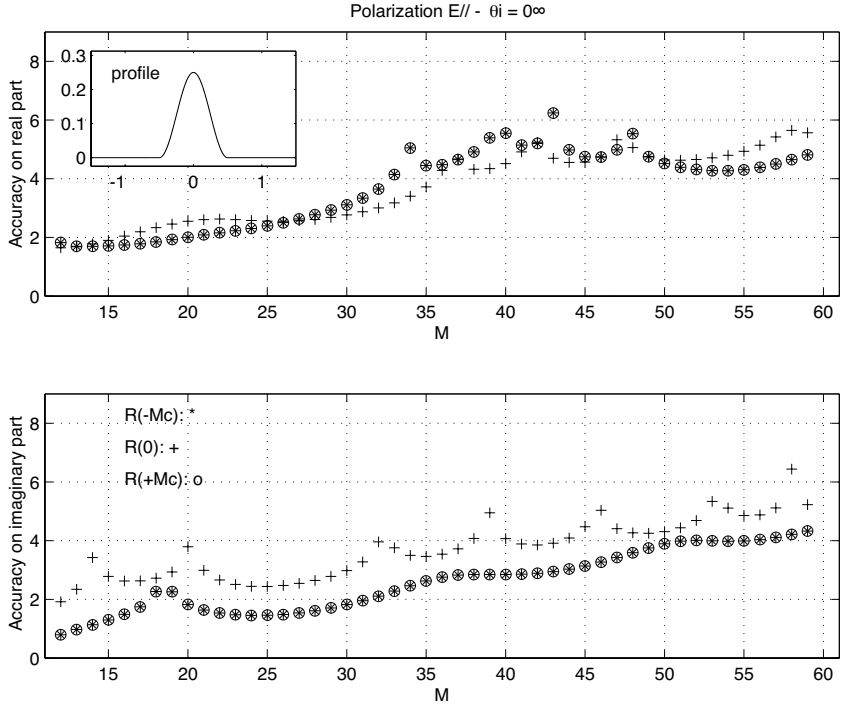

Figure 2. Accuracy on the real and imaginary parts of coefficients $R_0(M)$ and $R_{\pm M_C}(M)$ for the first profile referred to in Subsection 5.1 with $h = \lambda/8,\ D = l = \lambda,\ M_C = 12,\ \theta_i = 0°$ and with $E_{\|}$ polarization.

With M_C fixed, the integer part of $\Delta R_n(M, M_C)$ gives the number of unchanged digits when going from $M-1$ to M. This formula can also be applied to the real or imaginary part and modulus or phase of scattering coefficients R_n. Convergence is ensured if $\Delta R_n(M, M_C)$ is a monotonic increasing function of M. For M fixed, a similar error measure can obviously be obtained over intervals of M_C.

For a (M, M_C) pair, ΔP defines the accuracy on the power balance (8) and its integer part gives the number of significant digits common to P_d and P_c.

Figure 2 gives the accuracy on the real and imaginary parts of Rayleigh amplitudes R_0 and $R_{\pm \mathrm{M_C}}$ as a function of M for the profile $a(x) = h(\cos(\frac{2\pi x}{D}) + 1)$, with $h = \lambda/8$ and $D = \lambda$. This surface is a protrusion of height $\lambda/4$, of width $l = \lambda$, symmetrical relative to the Oy axis and illuminated by a $E_{\|}$ polarized plane wave under incidence $\theta = 0°$. The interval $[-k; +k]$ is described by 25 pulses ($M_C = 12$).

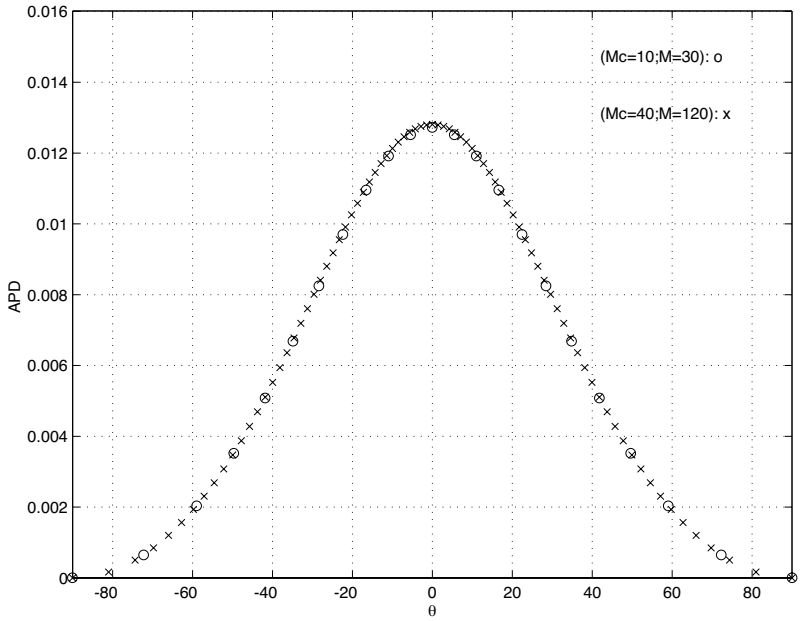

Figure 3. Angular power density (APD) for the first profile referred to in Subsection 5.1 with $(M_C; M) = (10; 40)$ and $(M_C; M) = (40; 120)$.

The convergence of results is satisfactory. For $M > 30$, the errors (36) are less than 10^{-2}. In fact, this accuracy is obtained on the $2M_C + 1$ coefficients R_n describing the far field. For $M > 30$ and $M_C = 12$, formula (35) gives $\alpha_{\max} \geq 2.4\,k$. For these values, the evanescent field is sufficiently well described for a good accuracy on the propagating field to be ensured. Figure 2 shows that $\Delta R_{+M_C} = \Delta R_{-M_C}$. In fact, for any M and n, the relative error, in absolute value, between R_{+n} and R_{-n} is less than 10^{-12}. As to the symmetric of this profile illuminated in normal incidence, the scattering pattern is symmetrical with respect to $\theta = 0°$.

Figure 3 gives the angular power density for $M_C = 10$ and $M_C = 40$ with $M = 3M_C$. The two curves are superimposed. The value of M_C depends on the lobe width of the scattering pattern. M_C sets the spectral resolution $\Delta\alpha$ and consequently, the angular resolution. One should increase the cut-off integer value for describing narrow lobes. For the profile under consideration here, the scattering pattern has one lobe with 3 dB width of 50 degrees. In this case, $M_C = 10$ is sufficient.

Figure 4 shows the error $\Delta P(M = 3M_C, M_C)$ as a function of

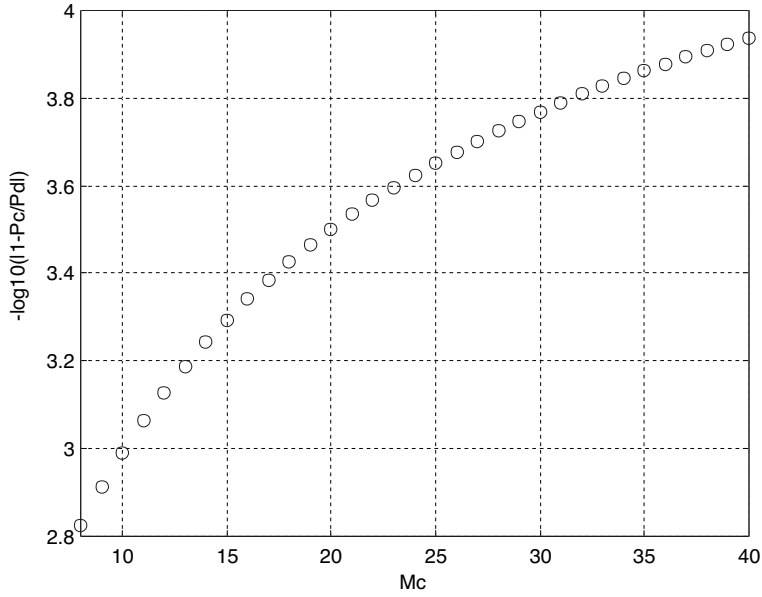

Figure 4. Accuracy $\Delta P(M_C)$ for the first profile referred to in subsection 5.1.

M_C. With $M = 3M_C$, $\alpha_{\max} = 3k$. This value ensures that coupling between the evanescent and propagating fields is well analyzed. For a high enough $\alpha_{\max}$ value, the accuracy on scattering coefficients and on the power balance increases with M_C. For instance, with $M_C = 10$, $\Delta P = 2.8$ and $M_C = 40$, $\Delta P = 3.95$.

Figure 5 gives the accuracy on the real and imaginary parts of $R_0(M)$ and $R_{-M_C}(M)$ for the profile $a(x) = h(\cos(\frac{2\pi x}{D}) + 1)$ illuminated in $H_{\parallel}$ under $\theta = 30°$, with $h = -\lambda/2$, $D = l = \lambda$ and $M_C = 18$. In comparison with the previous case, the convergence of results is slower. The errors are less than 10^{-2} from $M > 108$, i.e., from $\alpha_{\max} \geq 6.1k$ instead of $\alpha_{\max} \geq 2.4k$. The surface is a groove of depth λ. With such a depth, a good description of the scattered field inside and outside the groove requires a large number of evanescent waves with a large propagation constant in the Ox direction. To illustrate this fact, figure 6 shows the evolution of the normalized angular power density as a function of truncation order. The first four scattering patterns are given for $M = 18, 36, 72, 108$, i.e., for $\alpha_{\max} = k, 2k, 4k, 6k$. The differences are substantial. With $M = 108, 144$ and 180, i.e., with $\alpha_{\max} = 6k, 8k$ and 10k, the diagrams are superimposed. The

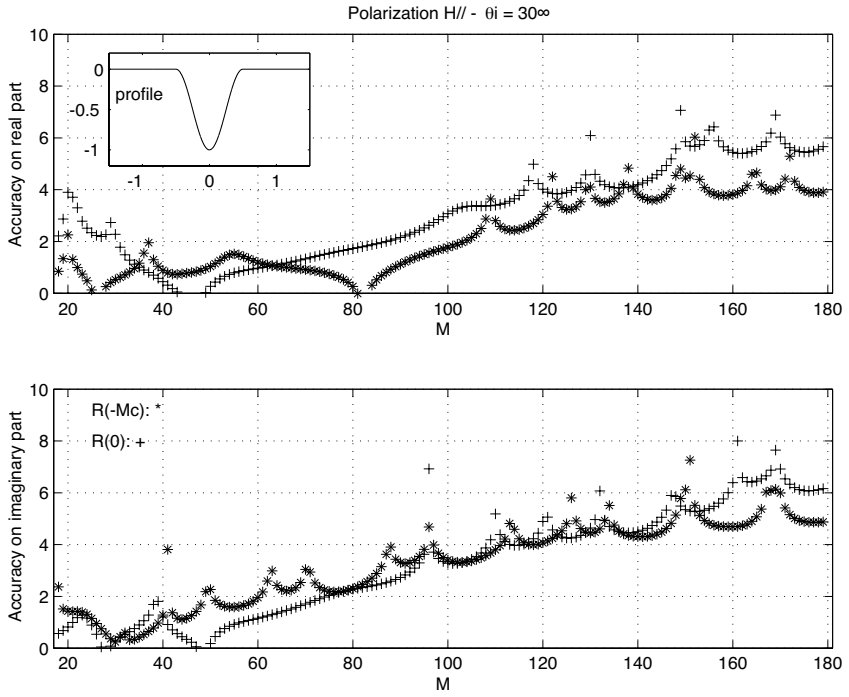

Figure 5. Accuracy on the real and imaginary parts of coefficients $R_0(M)$ and $R_{-M_C}(M)$ for the second profile referred to in Subsection 5A with $h = -\lambda/2,\ D = l = \lambda,\ M_C = 18,\ \theta_i = 30°$ and with $H_{\|}$ polarization.

differences are minor from $\alpha_{\max} \geq 6k$. In practice, as for diffraction gratings, the value of $\alpha_{\max}$ increases with the perturbation amplitude to wavelength ratio.

5.2. Comparison with the Exact Results for Schwartz Profiles

The profiles under consideration here are described by the following Schwartz function:

$$a(x) = 0 \quad \text{if} \quad x \notin [-l/2; 1/2]$$

$$a(x) = h \exp\left(b - \frac{bl^2}{l^2 - 4x^2}\right) \quad \text{if} \quad x \in [-l/2, -l/2]$$

$$\text{with} \quad l = 4\mu m \quad \text{and} \quad b = 3$$

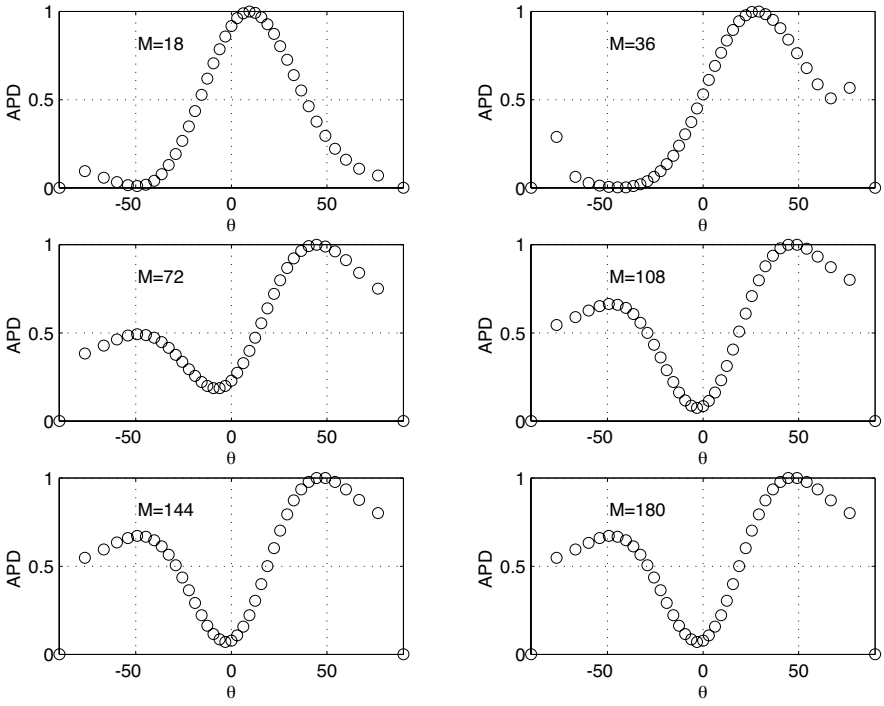

Figure 6. Normalized angular Power density for the second profile referred to in Subsection 5.1 with $M = 18, 36, 72, 108, 144$ and 180.

Figure 7 shows the scattering patterns for $E_{\parallel}$ polarized surfaces under $\theta = 0°$. The left side of the figure corresponds to $\lambda = 1\,\mu$m and the right side, to $\lambda = 4\,\mu$m. Height h varies from $0.1\,\mu$m (top) to $0.4\,\mu$m (middle) and finally $1\,\mu$m (bottom). Table 1 gives the highest directivity $D = \max(dP_d(\theta))/P_d$ of these surfaces in $E_{\parallel}$ and $H_{\parallel}$ polarizations. The profile appears to be wider for a wavelength of $\lambda = 1\,\mu$m and consequently, is more directional. As the height increases, secondary lobes appear in the scattering pattern associated with $\lambda = 1\,\mu$m.

Results are reliable. Errors on the power balance given in Table 1 are smaller than 10^{-2} and agreement with the curves of reference 14 (figure 8) is good.

Table 1. Accuracy ΔP and directivity D in $E_\parallel$ and $H_\parallel$ polarizations for the Schwartz profiles referred to in Subsection 5B.

		$h = 0.1\,\mu$m $(M_C; M) = (20; 60)$	$h = 0.4\,\mu$m $(M_C; M) = (24; 72)$	$h = 1\,\mu$m $(M_C; M) = (30; 120)$
$\lambda = 1\,\mu$m	$\Delta P_{E_\parallel}$	2.96	3.02	2.68
	$\Delta P_{H_\parallel}$	2.91	2.81	2.65
	$D_{E_\parallel}$	2.25	1.63	1.28
	$D_{H_\parallel}$	2.18	1.57	1.41
$\lambda = 4\,\mu$m	$\Delta P_{E_\parallel}$	3.73	3.61	3.12
	$\Delta P_{H_\parallel}$	3.55	4.93	3.23
	$D_{E_\parallel}$	0.778	0.761	0.692
	$D_{H_\parallel}$	0.485	0.438	0.373

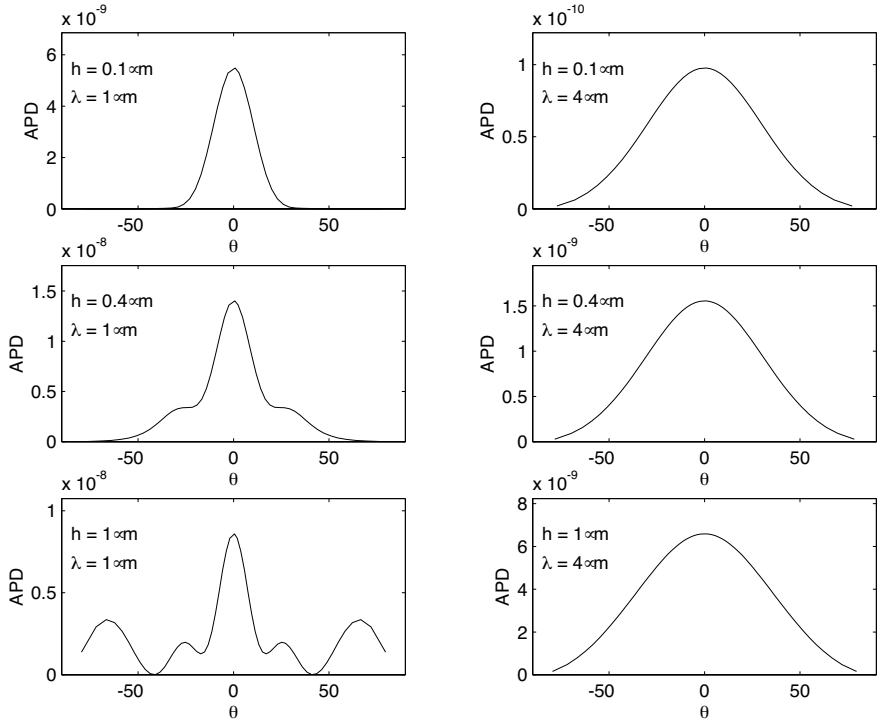

Figure 7. Angular Power density for $E_\parallel$ polarized Schwartz profiles referred to in Subsection 5.2 with $\theta = 0°$.

6. CONCLUSION

A differential method given the field scattered by a plane with a 1-dimensional local perturbation illuminated by a plane wave has been explained in details. This method is based on a covariant formulation of Maxwell's equations written in the translation system. The covariant components of the electric and magnetic fields fulfil an eigenvalue system and can be expanded as a linear combination of eigensolutions satisfying the outgoing wave condition. Their amplitudes are found by solving the boundary conditions. Above the deformation, the Rayleigh integral is valid and becomes identified with the Oz covariant component of the scattered field. This continuity relation allows the asymptotic field and the angular power density to be obtained. All solving steps are performed in the spectral domain with a method of moments using pulses as basis and weighting functions.

Numerical results depends on the truncation order M and the cut-off integer M_C. The width $\Delta\alpha$ of basis and weighting function $\hat{b}_q(\alpha)$ is in inverse proportion to M_C. As M_C increases, $\Delta\alpha$ decreases and the approximation of the Fourier transform of scattered field in a series of basis functions becomes more accurate. With the M^{th}-truncated approximation, the scattering matrix $\mathbf{L}$ is $4M + 2$-dimensional. It is proven that r_n and $-r_n$ are eigenvalues of $\mathbf{L}$ and that, consequently, among the $4M + 2$ eigenfunctions, $2M + 1$ of them correspond to outgoing waves, and as many to incoming waves. For a plane surface with a local deformation, it can be noted numerically, that $2M_C + 1$ outward-going wave functions characterize propagating waves and $2M - 2M_C$, evanescent waves. The proportion of the evanescent wave functions is larger when $M - M_C$ increases, so that the near field coupling phenomena are better described.

Through several examples, we have shown that the accuracy on the spectral amplitudes and on the power balance increases with M and M_C. The numerical stability of the method is ensured. Moreover, the comparison with the results obtained by a rigorous method is satisfying for different Schwartz (and canonical) profiles.

The next step of our work will to extend the method to a conical incidence [19] and afterwards, to study the scattering of a two-dimensional beam of incoming plane waves by a cylindrical rough surface in the resonance region (As a first approximation, a ploughed field [20] can be depicted by a cylindrical surface, and the radiation law of an antenna by a two-dimensional beam).

APPENDIX A. COEFFICIENTS OF THE SCATTERING MATRIX

Substituting expressions $\hat{F}(\alpha,u)$, $\hat{G}(\alpha,u)$, $\hat{c}(\alpha)$ and $\hat{d}(\alpha)$ into system (12) with their respective series expansions (13) and (14), we obtain system (A1).

$$\begin{aligned}\frac{1}{jk}\sum_{q=-\infty}^{q=+\infty}\frac{dF_q(u)}{du}\hat{b}_q(\alpha) &= \frac{-1}{2\pi k}\sum_{q=-\infty}^{q=+\infty}\sum_{l=-\infty}^{l=+\infty}F_q(u)d_l\hat{M}_{ql}^{(1)}(\alpha)\\ &\quad+\frac{1}{2\pi}\sum_{q=-\infty}^{q=+\infty}\sum_{l=-\infty}^{l=+\infty}G_q(u)c_l\hat{M}_{ql}^{(0)}(\alpha)\\ &\quad-\sum_{q=-\infty}^{q=+\infty}G_q(u)\hat{b}_q(\alpha) \qquad \text{(A1a)}\end{aligned}$$

$$\begin{aligned}\frac{1}{jk}\sum_{q=-\infty}^{q=+\infty}\frac{dG_q(u)}{du}\hat{b}_q(\alpha) &= \frac{-\alpha}{2\pi k^2}\sum_{q=-\infty}^{q=+\infty}\sum_{l=-\infty}^{l=+\infty}F_q(u)c_l\hat{M}_{ql}^{(1)}(\alpha)\\ &\quad-\frac{k^2-\alpha^2}{k^2}\sum_{q=-\infty}^{q=+\infty}F_q(u)\hat{b}_q(\alpha)\\ &\quad-\frac{\alpha}{2\pi k}\sum_{q=-\infty}^{q=+\infty}\sum_{l=-\infty}^{l=+\infty}G_q(u)d_l\hat{M}_{ql}^{(0)}(\alpha) \qquad \text{(A1b)}\end{aligned}$$

The convolutions $\hat{M}_{ql}^{(0)}(\alpha)$ and $\hat{M}_{ql}^{(1)}(\alpha)$ are centered on α_{q+l} and have a support of width $2\Delta\alpha$.

$$\hat{M}_{ql}^{(0)}(\alpha) = \int_{-\infty}^{+\infty}\hat{b}_q(\gamma)\hat{b}_l(\alpha-\gamma)d\gamma \qquad \text{(A2a)}$$

$$\hat{M}_{ql}^{(1)}(\alpha) = \int_{-\infty}^{+\infty}\gamma\hat{b}_q(\gamma)\hat{b}_l(\alpha-\gamma)d\gamma \qquad \text{(A2b)}$$

Projecting system (A1) onto each basis function $\hat{b}_q(\alpha)$, a set of differential equations relating coefficients $F_q(\alpha)$ and $G_q(\alpha)$ is obtained (A3).

$$\frac{1}{jk}\frac{dF_m(u)}{du} = \frac{-1}{2\pi k}\sum_{q=-\infty}^{q=+\infty}\sum_{l=-\infty}^{l=+\infty}F_q(u)d_lT_{mql}^{(11)}$$

$$+\frac{1}{2\pi}\sum_{q=-\infty}^{q=+\infty}\sum_{l=-\infty}^{l=+\infty} G_q(u)c_l T_{mql}^{(12)} - G_m(u) \tag{A3a}$$

$$\frac{1}{jk}\frac{dG_m(u)}{du} = \frac{-1}{2\pi k^2}\sum_{q=-\infty}^{q=+\infty}\sum_{l=-\infty}^{l=+\infty} F_q(u)c_l T_{mql}^{(21)} - (1-P_m)F_m(u)$$
$$-\frac{1}{2\pi k}\sum_{q=-\infty}^{q=+\infty}\sum_{l=-\infty}^{l=+\infty} G_q(u)d_l T_{mql}^{(22)} \tag{A3b}$$

with

$$T_{mql}^{(11)} = \left\langle \hat{b}_m(\alpha); \hat{M}_{ql}^{(1)}(\alpha) \right\rangle \tag{A4a}$$

$$T_{mql}^{(12)} = \left\langle \hat{b}_m(\alpha); \hat{M}_{ql}^{(0)}(\alpha) \right\rangle \tag{A4b}$$

$$T_{mql}^{(21)} = \left\langle \hat{b}_m(\alpha); \alpha\hat{M}_{ql}^{(1)}(\alpha) \right\rangle \tag{A4c}$$

$$T_{mql}^{(22)} = \left\langle \hat{b}_m(\alpha); \alpha\hat{M}_{ql}^{(0)}(\alpha) \right\rangle \tag{A4d}$$

and

$$P_m = \left\langle \hat{b}_m(\alpha), \frac{\alpha^2}{k^2}\hat{b}_m(\alpha) \right\rangle = \frac{\left(\alpha_m + \frac{\Delta\alpha}{2}\right)^3 - \left(\alpha_m - \frac{\Delta\alpha}{2}\right)^3}{3\Delta\alpha k^2} \tag{A5a}$$

Taking expressions of α_m and $\Delta\alpha$ (Eq. 15) into account, P_m can be written as follows:

$$P_m = \frac{12m^2+1}{3(2M_c+1)^2} \tag{A5b}$$

$[\alpha_{m-1/2};\alpha_{m+1/2}]$ is the support of $\hat{b}_m(\alpha)$ and $[\alpha_{q+l-1};\alpha_{q+l+1}]$ is the support of $\hat{M}_{ql}^{(0)}(\alpha)$ and $\hat{M}_{ql}^{(1)}(\alpha)$. Consequently, $T_{mql}^{(ij)}$ is non zero only for $m = q+l\pm 1$ and $m = q+l$. Considering $T_{mql}^{(ij)}$ values of Table 2 in the double summation, system (A3) has the form:

$$\frac{1}{jk}\frac{dF_m(u)}{du} = \sum_{q=-\infty}^{q=+\infty} L_{mq}^{(11)}F_q(u) + \sum_{q=-\infty}^{q=+\infty} L_{mq}^{(12)}G_q(u) \tag{A6a}$$

$$\frac{1}{jk}\frac{dG_m(u)}{du} = \sum_{q=-\infty}^{q=+\infty} L_{mq}^{(21)}F_q(u) + \sum_{q=-\infty}^{q=+\infty} L_{mq}^{(22)}G_q(u) \tag{A6b}$$

Table 2. Coefficient values $T_{mql}^{(ij)}$.

	$m = q + l - 1$	$m = q + l$	$m = q + l + 1$
$T_{mql}^{(11)}$	$\frac{1}{8}$	$\frac{3}{4}$	$\frac{1}{8}$
$T_{mql}^{(12)}$	$\frac{1}{8}(\alpha_q - \frac{\Delta\alpha}{24})$	$\frac{3\alpha_q}{4}$	$\frac{1}{8}(\alpha_q + \frac{\Delta\alpha}{24})$
$T_{mql}^{(21)}$	$\frac{1}{8}(\alpha_m + \frac{\Delta\alpha}{24})$	$\frac{3\alpha_m}{4}$	$\frac{1}{8}(\alpha_m - \frac{\Delta\alpha}{24})$
$T_{mql}^{(22)}$	$\frac{\alpha_m\alpha_q + \frac{(\alpha_q - \alpha_m)\Delta\alpha}{3} - \frac{5\Delta\alpha^2}{48}}{8}$	$\frac{3\alpha_m\alpha_q + \frac{5\Delta\alpha^2}{48}}{4}$	$\frac{\alpha_m\alpha_q + \frac{(\alpha_m - \alpha_q)\Delta\alpha}{3} - \frac{5\Delta\alpha^2}{48}}{8}$

where coefficients $L_{mq}^{(ij)}$ of the scattering matrix are defined as follows:

$$L_{mq}^{(11)} = \frac{-1}{2\pi k}\frac{\Delta\alpha}{8}\left\{\left(\alpha_q - \frac{\Delta\alpha}{3}\right)d_{m+1-q} + 6\alpha_q d_{m-q} + \left(\alpha_q + \frac{\Delta\alpha}{3}\right)d_{m-1-q}\right\} \tag{A7a}$$

$$L_{mq}^{(12)} = \frac{1}{2\pi}\frac{\Delta\alpha}{8}\left(c_{m+1-q} + 6c_{m-q} + c_{m-1-q}\right) - \delta_{m,q} \tag{A7b}$$

$$\begin{aligned} L_{mq}^{(21)} = {} & (P_m - 1)\delta_{m,q} - \frac{1}{2\pi k^2}\frac{\Delta\alpha}{8}\left\{\alpha_m\left(c_{m+1-q} + 6c_{m-q} + c_{m-1-q}\right)\alpha_q\right. \\ & + \frac{\Delta\alpha}{3}\left(c_{m+1-q} - c_{m-1-q}\right)\alpha_q - \frac{\Delta\alpha}{3}\alpha_m\left(c_{m+1-q} - c_{m-1-q}\right) \\ & \left. - \frac{5\Delta\alpha^2}{48}\left(c_{m+1-q} - 2c_{m-q} + c_{m-1-q}\right)\right\} \end{aligned} \tag{A7c}$$

$$L_{mq}^{(22)} = \frac{-1}{2\pi k}\frac{\Delta\alpha}{8}\left(\left(\alpha_m + \frac{\Delta\alpha}{3}\right)d_{m+1-q} + 6\alpha_m d_{m-q} + \left(\alpha_m - \frac{\Delta\alpha}{3}\right)d_{m-1-q}\right) \tag{A7d}$$

For a plane, $c_q = d_q = 0$, thus

$$L_{mq}^{(11)} = L_{mq}^{(22)} = 0; \quad L_{mq}^{(12)} = -\delta_{m,q}; \quad L_{mq}^{(21)} = (P_m - 1)\delta_{m,q} \tag{A8}$$

Combining (A5) and (A7), It may be shown that $F_m(u)$ and $G_m(u)$ are solutions of the linear second-order differential equation (A9):

$$\frac{d^2F_m(u)}{du^2} = k^2(1 - P_m)F_m(u) \tag{A9}$$

For a plane surface, the spatial dependence on u of eigenfunctions varies as $\exp(jkr_n u)$ with $r_n = \pm\sqrt{1 - P_n}$.

With an M^{th} order truncation, the scattering matrix $\mathbf{L}$ given by Eq. (A7) depends on $4M+3$ pairs of coefficients $(c_q; d_q)$. In order to obtain these coefficients, we consider the two following equations:

$$\begin{array}{l} c(x) - \dot{a}(x)d(x) = 0 \\ \dot{a}(x)c(x) + d(x) = \dot{a}(x) \end{array} \tag{A10}$$

After a Fourier transform of Eq. (A8), substituting functions $\hat{c}(\alpha)$ and $\hat{d}(\alpha)$ with their respective series expansions (14) and projecting onto basis functions, we obtain a set of equations relating coefficients c_q and d_q.

$$\begin{array}{l} \displaystyle\sum_{m=-M-1}^{m=M+1} \delta_{m,q} c_q + \sum_{m=-M-1}^{m=M+1} S_{mq} d_q \;=\; 0; \quad -M-1 \le q \le M+1 \\ \displaystyle\sum_{m=-M-1}^{m=M+1} S_{mq} c_q + \sum_{m=-M-1}^{m=M+1} \delta_{m,q} d_q \;=\; K_m \end{array} \tag{A11}$$

with

$$S_{mq} \;=\; \frac{j}{2\pi\Delta\alpha} \int_{-l/2}^{l/2} \left(I_{0q}(x) I_{1m}^{*}(x) - I_{1q}(x) I_{0m}^{*}(x) \right) a(x) dx \tag{A12a}$$

$$K_m \;=\; \frac{j}{\Delta\alpha} \int_{-l/2}^{l/2} I_{1m}^{*}(x) a(x) dx \tag{A12b}$$

Expressions of $I_{0m}(x)$ and $I_{1m}(x)$ are given in Subsection 4.5.

REFERENCES

1. Chandezon, J., D. Maystre, and G. Raoult, "A new theoritical method for diffraction gratings and its numerical application," *J. Optics (Paris),* Vol. 11, 235–241, 1980.
2. Elson, J. M., and R. H. Ritchie, "Photon interaction at a rough metal surface," *Phys. Rev.,* Vol. B4, 4129–4138, 1971.
3. Stratton, J. A., *Electromagnetic Theory,* McGraw-Hill, New York, 1941.
4. Nevière, M. and E. Popov, "New theoretical method for electromagnetic wave diffraction by a metallic or dielectric cylinder, bare or coated with a thin dielectric layer," *Journal Elect. Waves Appl.,* Vol. 12, 1265–1296, 1998.

5. Harrington, R. F., *Field Computation by Moment Methods,* Mc Millan, London, 1968.
6. Van Den Berg, P. M. and J. T. Fokkema, "The Rayleigh hypothesis in the theory of diffraction by a perturbation in a plane surface," *Radio Sci.,* Vol. 15, 723–732, 1980.
7. Millar, R. F., "The Rayleigh hypothesis and a related least-square solution to scattering problems for periodic surfaces and other scatterers," *Radio Sci.,* Vol. 8, 785–796, 1973.
8. Afifi, S., "Propagation et diffraction d'une onde électromagnétique dans des structures apériodiques," Ph.D. Dissertation, Université Blaise Pascal, Clermont-Ferrand, France, 1986.
9. Benali, A., J. Chandezon, and J. Fontaine, "A new theory for scattering of electromagnetic waves from conducting or dielectric rough surfaces," *IEEE Trans. Antennas Propagat.,* Vol. 40, No. 2, 141–148, 1992.
10. Guizal, B., G. Granet, and J. Chandezon, "Diffraction d'une onde électromagnétique par une surface apériodique," *OHD'97 symposium,* 264–266, Clermont-Ferrand, France, 1997.
11. Baudier, C. and R. Dusséaux, "Scattering of an $E_{\|}$-polarized plane wave by one-dimensional rough surfaces: Numerical applicability domain of a Rayleigh method in the far-field zone," *Journal of Elect. Waves and Appli.,* to be published.
12. DeSanto, J. A., "Exact spectral formalism for rough-surface," *J. Opt. Soc. Am. A,* Vol. 2, 2202–2207, 1989.
13. Maystre, D., "Electromagnetic scattering from perfectly conducting rough surfaces in the resonance region," *IEEE Trans. Antennas Propagat.,* Vol. 31, No. 6, 885–895, 1983.
14. Faure-Geors, H. and D. Maystre, "Improvement of the Kirchhoff approximation for scattering from rough surface," *J. Opt Soc. Am. A,* Vol. 6, 532–542, 1989.
15. Axline, R. M. and A. K. Fung, "Numerical computation of scattering from a perfectly conducting random surface," *IEEE Trans. Antennas Propagat.,* Vol. 26, No. 3, 482–488, 1978.
16. Li, L., "Multilayer-coated diffraction gratings: differential method of Chandezon et al. revisited," *J. Opt Soc. Am. A,* Vol. 11, 2816–2828, 1994.
17. Dusséaux, R., C. Faure, J. Chandezon, and F. Molinet, "New perturbation theory of diffraction gratings and its application to the study of ghosts," *J. Opt. Soc. Am. A,* Vol. 12, 1271–1282, 1995.
18. Dusséaux, R., P. Chambelin, and C. Faure, "Analysis of

rectangular waveguide H-plane junctions in nonorthogonal coordinate system," *Progress In Electromagnetic Research,* PIER 28, 205–229, 2000.

19. Popov, E. and L. Mashev, "Conical diffraction mounting. Generalization of a rigourous differential method," *J. Optics (Paris),* Vol. 17, No. 4, 175–180, 1986.
20. Zribi, M., V. Ciarletti, and O. Taconet, "Validation of a rough surface model based on fractional brownian geometry with SIRC and ERSAME radar data over Orgeval," *Remote Sens. Environ.,* Vol. 72, 65–72, 2000.